Supporting Information

Guided assembly and patterning of intrinsically fluorescent amyloid fibers with long-range order

*Lisa Hecker, Wenyu Wang, Ioanna Mela, Saeed Fathi, Chetan Poudel, Giancarlo Soavi, Yan Yan Shery Huang, Clemens F. Kaminski**

* cfk23@cam.ac.uk

This PDF includes:

Supplementary Note 1: Fabrication of the material

Protein preparation

Bovine β-lactoglobulin (L2506), 1,1,1,3,3,3-hexafluoro-2-propanol (105228), and PEO (polyethylene oxide, Mw = 4000 kDa) were purchased from Sigma Aldrich. For monomerization, the lyophilised protein powder was dissolved at 10 mg/mL in HFIP using sequential ultrasonic treatment and vortex mixing followed by a visual inspection to ensure efficient solubilisation. HFIP was subsequently removed in a lyophiliser

(LyoQuest, Telstar) and the remaining protein powder was re-dissolved in milliQ water. The solution was centrifuged at 12,000 g and the supernatant filtered through a 0.22 µm Millipore filter before being adjusted to pH 2 using 8M HCl. Samples prepared for electrospinning assembly were immediately transferred into a 1 mL syringe in the nearfield spinning setup or stored at -20°C. Solutions for control experiments with thermally induced fibrillation were incubated at 80°C for 2 hours and immediately cooled in an ice bath to quench the aggregation process. Polyethylene oxide was dissolved in milliQ water and transferred into a 10 mL syringe to be used as a shell-solution.

Electrospinning

The electrospinning setup used in this study has been described in detail by [1] and utilises a coaxial low-voltage electrospinning approach with additional mechanical stretching forces. The functional β-lactoglobulin core solution was passed through a fine needle with 100 µm inner diameter (World Precision Instrument) and subsequently combined with the supporting PEO shell solution in a blunt metallic tip (640 µm inner diameter, Adhesive Dispensing Ltd). Flow rates were adjusted to 40 µL/hr and 20 µL/hr for protein and polymer solutions respectively using two syringe pumps (World Precision Instruments, AL-1000) and left to stabilise for 10 minutes prior to the experiment. An automated xyz-stage (Thorlabs DDSM100, MLJ150/M) was used to adjust the working distance accurately and to collect the electrospun fibers in patterns on a heated, metallic collector plate with a speed of 350 mm/s. A custom-made voltage source was used to apply a potential between the blunt metallic tip and the collector

plate. For fabrication of substrate deposited fibers, the material of interest was placed on the collector plate next to a stack of glass slides with approximately 4 millimetre thickness (previously described as 'initiators') to enable the application of stretching forces and thinning of the fibers. The collector was heated to 80°C and voltages of 400-500 V were applied between the tip and the collector plate during the spinning process. Small rectangular mounts with a 30 mm gap were 3D printed for the fabrication of free-standing fibers. The mounts were placed onto the collector plate (20°C) and fibers collected between the two contacts without the use of additional initiators or electrical forces.

Supplementary Note 2: Structural characterisation of the material

Electron microscopy for analysis of the ultrastructure

Free standing fibers were measured using an environmental scanning electron microscope (FEI Philips XL30 FEG ESEM) at 800 V with ETD detector and magnifications of 300 - 5000. Average fiber diameters were determined by measuring 100 fibers selected from different mounts. For higher resolution images, fibers were deposited onto filter paper, plunge-frozen, freeze-dried, iridium coated and subsequently sliced and mounted upright in the microscope (FEI Verios 460) for cross-section imaging. Images were taken at 1kV on ETD and TLD detectors with magnifications of 200 – 30,000.

Fourier transform infrared spectroscopy for secondary structure analysis

FTIR spectra for characterisation of secondary structures were recorded at room temperature on a Spotlight 400N (Perkin Elmer). Background spectra were recorded between 600 cm^{-1} and 4000 cm^{-1} and subtracted from the scan for each sample. Samples for FTIR analysis were prepared by repeated deposition of fibers onto a glass until a dense, multiple layer thick pattern was formed. Fibers were subsequently scratched off the glass to form a fiber mat that could be mounted into the sample holder of the spectrometer. Test tube grown fibers were lyophilised after quenching of the aggregation process and measured as powder.

Supplementary Note 3: Mechanical characterisation of the material

AFM nanoindentation to estimate the material's Young's modulus

β-lactoglobulin monomers, oligomers and fibrils formed in the test tube were diluted to 0.1 mg/mL, deposited onto cleaved mica or cleaned glass slides and incubated at room temperature for 15 minutes. Samples were subsequently washed with milliQ water and air dried before being imaged on a Bruker Bioscope. Electro spun fibers were printed onto mica or glass slides and imaged on the same instrument.

For topology measurements, the instrument was operated in tapping mode in air using silicone nitride probes (SCANASYST-AIR, Bruker) with a nominal resonant frequency of 70 kHz, a spring constant of 0.4 Nm^{-1} and A nominal tip radius of 2 nm. Images were collected at a scan rate of 1.5 Hz and flattened if required using Bruker's NanoScope analysis V1.4 software.

Nanoindentation measurements were performed on the same instrument operating in PeakForce tapping mode in air using silicone probes (RTESPA-150, Bruker) with a resonant frequency of 150 kHz, a spring constant of 5 Nm^{-1} and a nominal tip radius of 8 nm. Prior to image collection, calibration measurements were performed. The cantilever spring constants were determined with a thermal noise method implemented in the nanoscope software and a contact calibration was performed on a hard substrate (SiO2, 2.5 MPa). The tip radius was determined using a tip-sample convolution method using the recorded calibration image with known modulus and quantitative image analysis was performed using the NanoScope analysis software. Young's modulus and stiffness values were estimated using the acquired force–distance curves at each point and fitting it with a cone-sphere or Sneddon model using the tip size, shape and deflection sensitivity obtained from the calibration measurements and a Poisson ratio σ of 0.3 as a reasonable guess [2] for fibrils. Values quoted are the average of multiple areas on different fibers/ samples.

Stress-Strain measurements on individual fibers

Stress-strain experiments were performed on individual fibers to estimate the material's tensile properties. A micro cantilever (World Precision Instruments, MF34G-5) was calibrated prior to the measurements and its force constant was estimated as pictured in figure S3A.

For this, a small force in form of the gravity of an 70% v/v ethanol droplet was applied to the cantilever while recording its deflection. The force was calculated as the gravity of the ethanol droplet. The shape of the hanging droplet could be estimated as a

prolate ellipsoid. Thus, the force applied at the cantilever equals to the gravity of the droplet:

$$F = \rho g \cdot \frac{4}{3}\pi a b^2$$

Where ρ is the density of the ethanol, g is the gravitational constant, a and b are the axials of the ellipsoid that are extracted from the camera images. Monitoring the cantilever deflection with different sizes of ethanol droplets allowed for the recording of a calibration curve as shown in figure S3A (ii), in which the force applied at the tip of the cantilever is found to be proportional with the cantilever's deflection.

The calibrated cantilever was subsequently used to apply force to a free-standing hybrid fibre as shown in figure S3B. At the beginning, the tip of the cantilever was placed just at the middle point of a suspended fibre. Then, a linear translation stage was used to move the sample with respect to the cantilever in intervals of 100 μm, leading to deflections for both the cantilever (D) and the suspended fibre (d). This process was monitored on an optical microscope. The deflection of the cantilever was subsequently translated to force F from Figure S3A (ii).

Using this method, it is possible to estimate the stress of the fibre as the quotient of the force **F** at the probe and the cross-section area **A** of the fibre (assuming the fibre diameter is uniform during the process as ~ 1.8 μm), as well as the fiber's angle **α** :

$$stress = \frac{F}{2 \cdot \cos(\alpha / 2) \cdot A}$$

The strain of the fibers is calculated using their original length **L** (distance between the two initiators) and their displacement **D** by the pulling probe in each step as recorded by the microscope:

$$strain = \frac{2\sqrt{D^2 + (L/2)^2} - L}{L} \times 100\%$$

When plotted as stress-strain diagram, it is possible to estimate the material's Young's modulus from the linear part of the curve which equals the slope of this section of the graph.

Supplementary Note 4: Optical characterisation of the material

Fluorescence spectroscopy

Fluorescence emission spectra of the electrospun fibers, PEO polymer and test tube grown fibers were measured at 20°C using a custom-built imaging setup. For the excitation of the samples we used the second harmonic of a Ti:Sa laser (Coherent Chameleon) at a central wavelength of 365nm, pulse duration of approx. 200fs and repetition rate of 80MHz. The fluorescence spectra between 400nm and 650nm were measured with a nitrogen cooled CCD imaging spectrometer (Horiba iHR550).

Fluorescence Lifetime Measurements

Fluorescence lifetime images were acquired on a Leica SP5 laser-scanning microscope, which was equipped with a 40X/1.30 NA oil immersion objective (HC PLAPO CS2, Leica) and coupled to a Ti:Sapphire laser (Coherent Chameleon) producing femtosecond pulses at a repetition of 80 MHz. Two-photon excitation

wavelength was tuned to 740 nm and a short-pass 680-nm dichroic mirror was used to separate the fluorescence signal from the laser light. The intrinsic fluorescence associated with β-lactoglobulin was generated at the focal spot of the objective and was directed through a FF01-450/70 bandpass filter (Semrock, USA) onto a hybrid detector (HPM-100, Hamamatsu) connected to a TCSPC module (SPC-152N, Becker and Hickl GmBH, Germany) for time-resolved detection. For each 256x256 pixel FLIM image, an acquisition time of 2 minutes was used by integrating around 100 frames. Photobleaching was verified to be negligible during the experiment.

Supplementary Note 5: Influence of fiber architecture on the material's properties

Broad and 'flat' fibers lack a stable core formation

In this manuscript we demonstrate with several experimental methods that successful electrospinning results in the formation of µm thin, unbranched amyloid-hybrid fibers (see figures 2A&B(ii), S2).

However, 'flat' structures rather than cylindrical fibers are occasionally observed, especially for long, surface deposited samples (see figures 1D (i) sides or 2B (iv)).

We hypothesize that these structures result from problems with a stable core formation e.g. due to inhomogeneous conditions in the solution. Our hypothesis is strengthened by fluorescence lifetime measurements on such broad fibers which reveal long lifetimes that match those of the oligomeric rather than amyloidogenic proteins (figure

4C (iii & iv). We therefore hypothesize that the flat structures correspond to a monomeric or oligomeric protein-PEO mixture which results from the lack of core confinement during the spinning process and the failure of stable core formation. To confirm that the flat structures only contain unaggregated protein and differ from fibers of blended PEO and amyloid aggregates, we produced mixed phase fibers with an amyloid-PEO mixture. A FLIM analysis of such blend fibers revealed significantly shorter lifetimes than those of the flat, oligomeric constructs as well as differences to the core-shell fibers (figure S5A).

Amyloid-PEO blend vs core-shell architecture

The very distinct fluorescence lifetimes of the blend fibers led to further investigations of this sample architecture. Notably, the blend lifetimes resemble those of high viscosity, (hydro)gel-like β-lactoglobulin fibril networks which form upon prolonged incubation times for high concentrations of the protein in the test tube [3]. This is in line with Munishkina et al. [4], who found that the contact with PEO accelerates the aggregation of proteins into amyloids and the formation of (hydro)gels. Our mixed phase architecture therefore seems to be influenced by the direct interaction of protein and PEO, leading to a hydrogel-like fiber with lower protein fibril density, looser packing of the amyloids and consequently different material properties.

This is confirmed by a comparison of the mechanical properties of blended and core-shell fibers which is presented in figure S5B. Blend fibers were found to provide high elastic moduli but rupture quickly, while a core-shell architecture prevents the rupture

of fibers and combines the high moduli of amyloids in its functional core with the flexibility of the surrounding PEO shell.

Compared to existing amyloid materials, the core-shell architecture permits the condensation of densely packed amyloid fibrils. Due to the rapid solvent evaporation and the low mobility of the high molecular weight PEO, there is limited mixing between the core and the shell phase and little dilution of the core protein phase by the shell phase. In addition to that, the small fiber diameter imposes confinement at the micrometer length scale, which forces the assembly and aggregation of amyloid fibrils into higher densities per unit volume than is possible with other existing fabrication methods (figure 5).

Supplementary Note 6: Discussion on possible applications for the material

Amyloids, as well as the developed hybrid material, share many properties of silk. This exceptionally strong biomaterial is of great interest for structural applications, but not easy to produce and structure. Like silk, the hybrid fiber patterns presented in this study could find application as scaffolds for cell guiding and patterning [5], as wound dressings in tissue and for stem cell engineering [6]. The strength of the material and its ability to carry substantial loads are demonstrated in figure 3c and the supplementary video 1 and highlight the applicability of the material to structural and mechanical applications.

With its optical properties, the material also demonstrates its use to produce patterned light sources. The ease of amyloid functionalization enables to tune emission wavelengths [7] and light guiding in amyloid-like fibers has previously been reported [8]. In combination with our ability to pattern the fibers on a macroscale, this opens possibilities for the use of the material as photodetectors, light harvesting devices or fluorescent concentrators.

We have performed preliminary work on light guiding in our electro spun amyloid fibres which is presented in figure S6. On localised excitation of a fibre with a UV laser spot, the generated fluorescence is seen to be guided through the fibre over long distances. In combination with cell patterning for example on fibre structures one could envisage patterned optical activation of biological or physical functions, for example through the use of photoactivatable fluorescent proteins or through use of optogenetic switches.

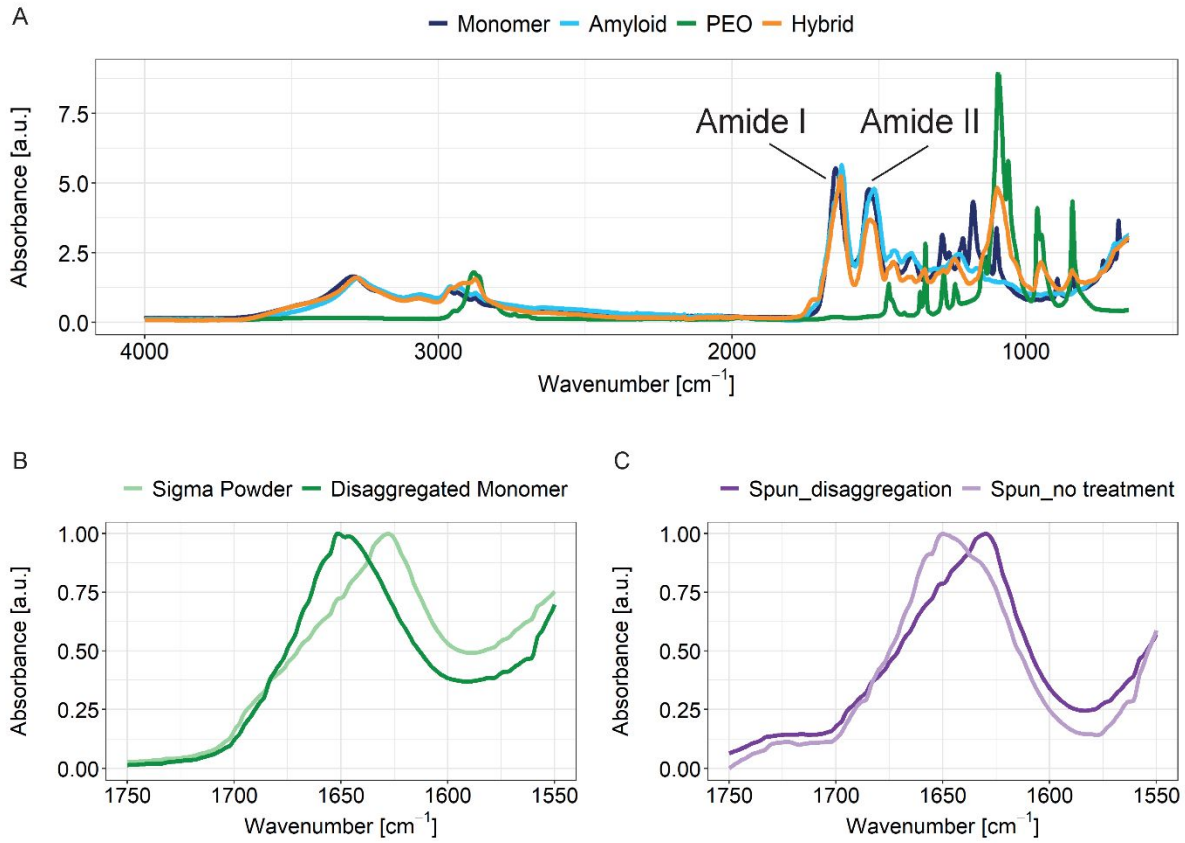

Figure S1: FTIR analysis of the materials. A: The hybrid material spectrum (orange) shows two protein characteristic peaks near 1630 cm^{-1} (Amide I) and 1535 cm^{-1} (Amide II) which are not present in pure PEO fibers. The amide I area between 1700 cm^{-1} and 1600 cm^{-1} is used for secondary structure analysis throughout the manuscript. B: FTIR spectra of lyophilised β-lactoglobulin after disaggregation (dark green) shows differences to the partly aggregated powder purchased from Sigma (light green). C: Hybrid fibers spun from disaggregated proteins have a different composition of secondary structure elements than those produced directly from the purchased powder.

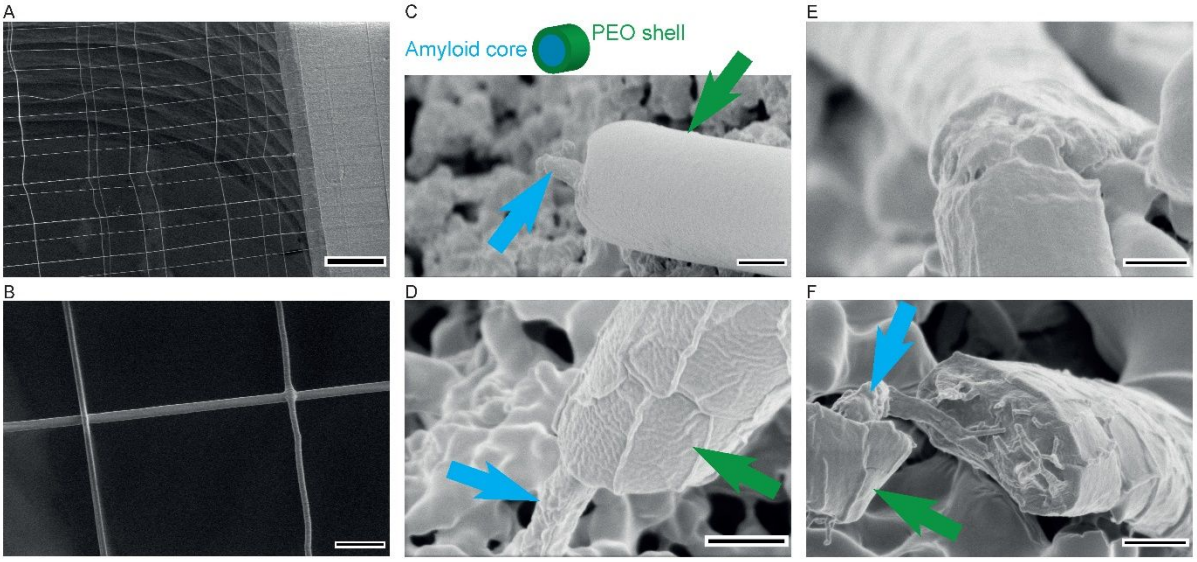

Figure S2: Characterisation of the material's ultra-structure using electron microscopy. A&B: Environmental SEM enables the imaging of free-standing fibers which can be created as crossed patterns over several mm length. Scale bars 200 µm and 10 µm. C-E: High resolution images of paper deposited fibers confirm a core-shell structure of the material, while the fiber core in F collapses into a flat structure without continuous core. Scale bars 500 nm.

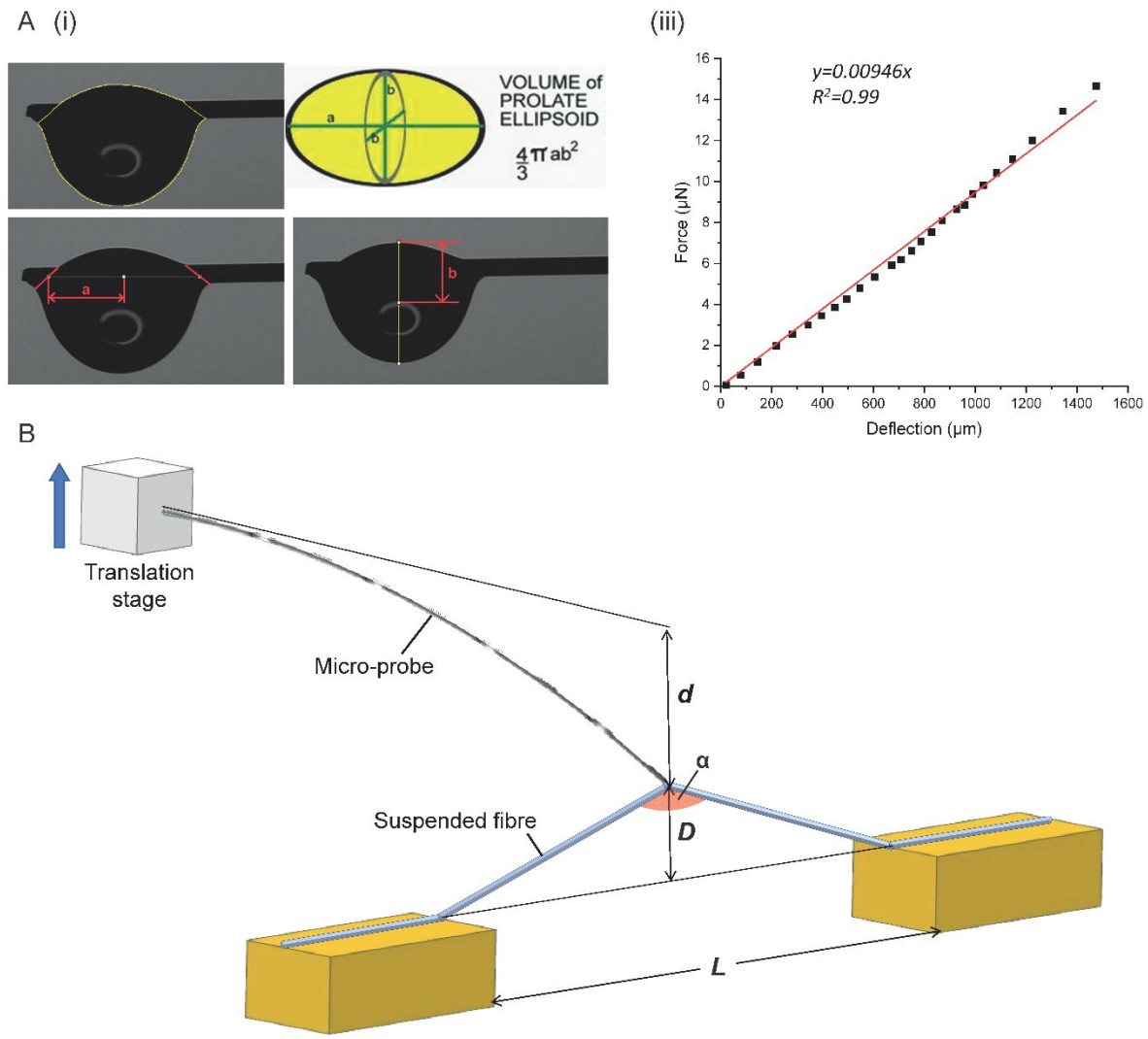

Figure S3: Procedure of stress-strain measurements on the single fiber scale. A: A micro cantilever is calibrated by measuring its deflection upon force in form of a small droplet. As the droplet evaporates, the force on the cantilever and its deflection decrease, which enables the recording of a calibration curve (ii). B: The cantilever is brought into contact with a free-standing fibre and subsequently moved stepwise by a defined distance. The deflection of the fibre is recorded for each step and used to calculate the materials strain while the known step size and force constant of the cantilever provide the corresponding stress values.

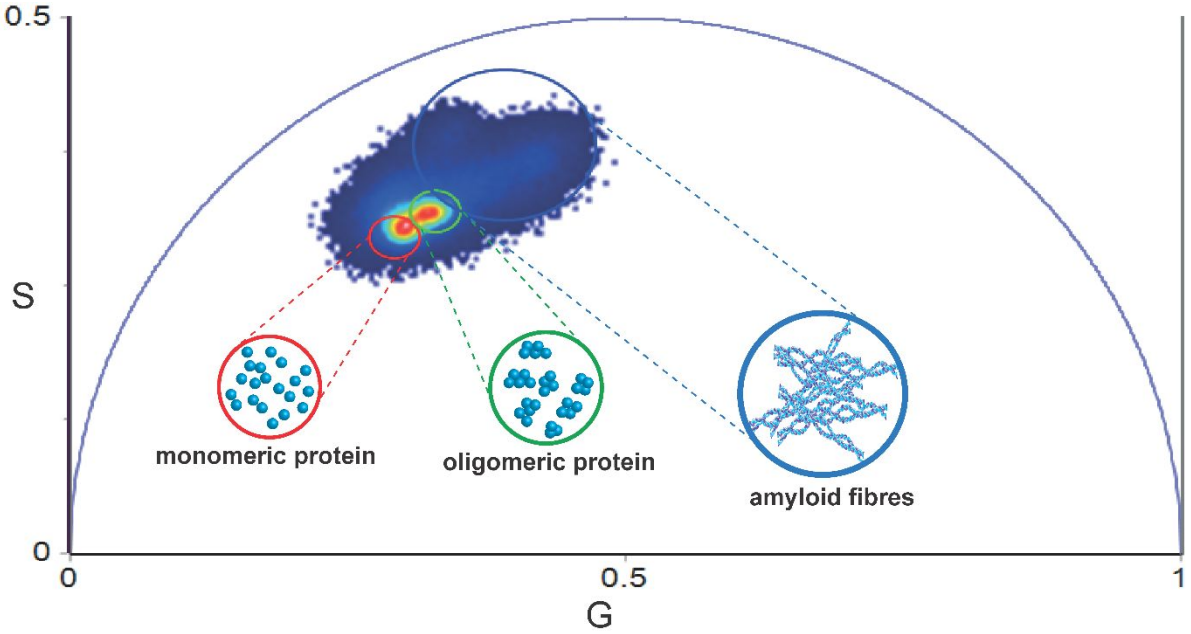

Figure S4: Phasor plot analysis of fluorescence lifetimes. Observed lifetime decays are multi-exponential and confirm structural differences between hybrid fibers, protein monomers and oligomers. Aggregated components show a wider spread of lifetimes while monomeric and oligomeric components are highly concentrated in small areas. Overall, lifetimes were observed to reduce with increase in aggregation.

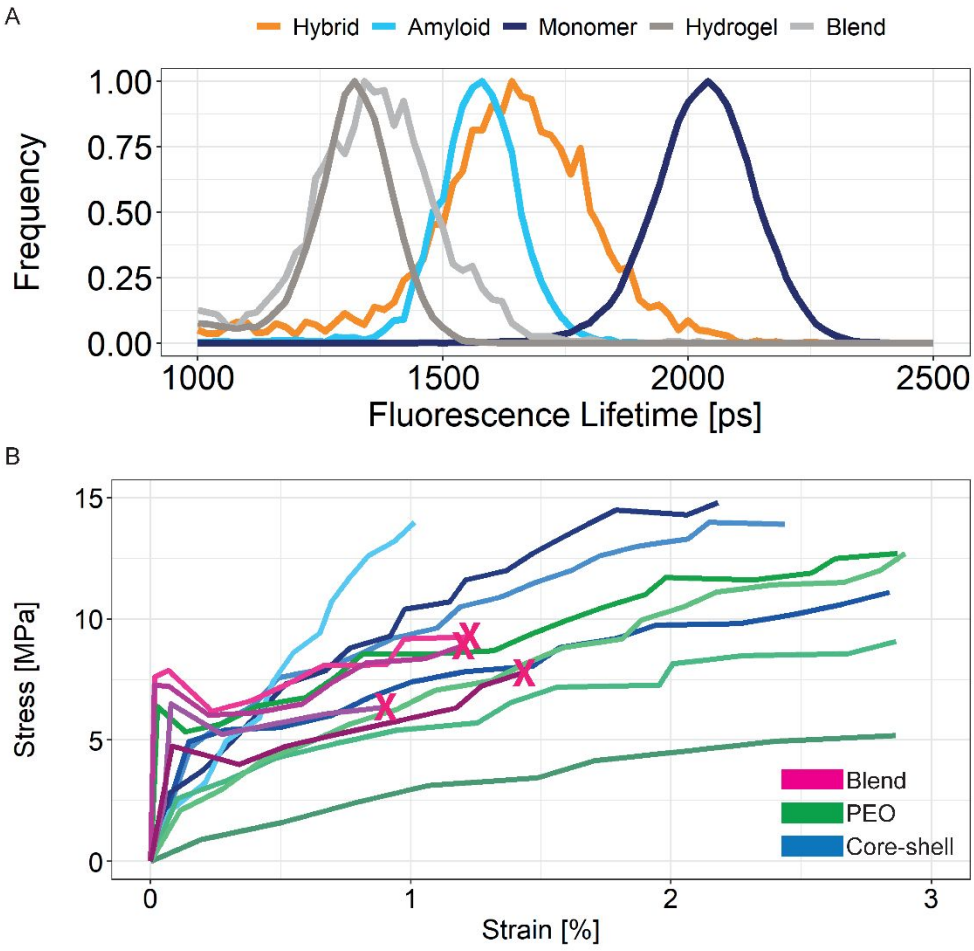

Figure S5: Material properties vary with changing fiber architecture. A: Core-shell structures (orange) yield fibers with fluorescent lifetime characteristics between oligomeric (dark blue) and aggregated amyloid protein (light blue). In comparison, electro spun amyloid-PEO blend fibers (light grey) show significantly shorter lifetimes that are more similar to amyloid hydrogel assemblies (dark grey). B: Fibers composed of an amyloid-PEO blend (magenta) show high elastic moduli but rupture easily, indicated by the magenta X. In comparison, core-shell structures (blue) seem to combine the high elastic moduli of amyloids in their core with the flexibility of the surrounding PEO shell. A rupture was not observed for these fibers.

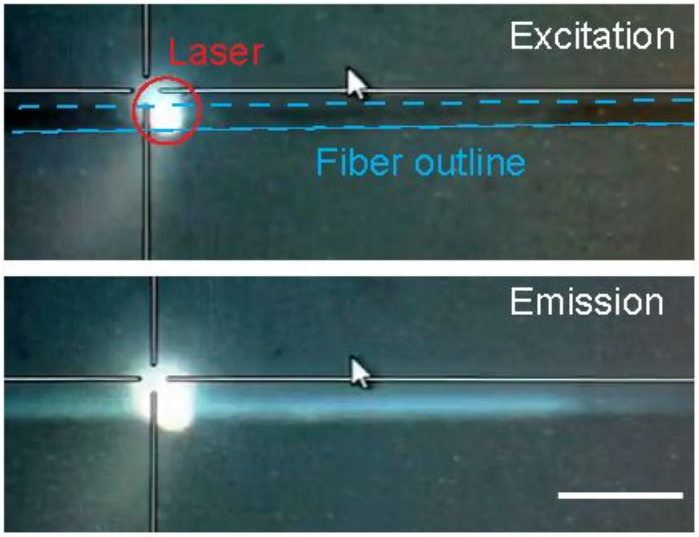

Figure S6: Localised excitation of fluorescence in the amyloid fibre at a wavelength of 325 nm (top panel) yields to guided fluorescence emission in the fibre over long distances (bottom panel). Scale bar 20 µm

References

1. Li, X.; Li, Z.; Wang, L.; Ma, G.; Meng, F.; Pritchard, R. H.; Gill, E. L.; Liu, Y.; Huang, Y. Y. S. Low-Voltage Continuous Electrospinning Patterning. *ACS Appl. Mater. Interfaces* 2016, *8* (47), 32120–32131. https://doi.org/10.1021/acsami.6b07797.

2. Sweers, K.; van der Werf, K.; Bennink, M.; Subramaniam, V. Nanomechanical Properties of α-Synuclein Amyloid Fibrils: A Comparative Study by Nanoindentation, Harmonic Force Microscopy, and Peakforce QNM. Nanoscale Res. Lett. 2011, 6 (1), 270. https://doi.org/10.1186/1556-276X-6-270.

3. Bolisetty, S.; Harnau, L.; Jung, J. M.; Mezzenga, R. Gelation, Phase Behavior, and Dynamics of β-Lactoglobulin Amyloid Fibrils at Varying Concentrations and Ionic Strengths. Biomacromolecules 2012, 13 (10), 3241–3252. https://doi.org/10.1021/bm301005w.

4. Munishkina, L. A.; Ahmad, A.; Fink, A. L.; Uversky, V. N. Guiding Protein Aggregation with Macromolecular Crowding. Biochemistry 2008, 47 (34), 8993–9006. https://doi.org/10.1021/bi8008399.

5. Zhang, Q.; Zhao, Y.; Yan, S.; Yang, Y.; Zhao, H.; Li, M.; Lu, S.; Kaplan, D. L. Preparation of Uniaxial Multichannel Silk Fibroin Scaffolds for Guiding Primary Neurons. Acta Biomater. 2012, 8 (7), 2628–2638. https://doi.org/10.1016/J.ACTBIO.2012.03.033.

6. Mehrotra, S.; Chouhan, D.; Konwarh, R.; Kumar, M.; Jadi, P. K.; Mandal, B. B. Comprehensive Review on Silk at Nanoscale for Regenerative Medicine and Allied Applications. ACS Biomaterials Science and Engineering. American Chemical Society May 13, 2019, pp 2054–2078. https://doi.org/10.1021/acsbiomaterials.8b01560.

7. Ryu, J.; Lim, S. Y.; Park, C. B. Photoluminescent Peptide Nanotubes. Adv. Mater. 2009, 21 (16), 1577–1581. https://doi.org/10.1002/adma.200802700.

8. Li, Q.; Jia, Y.; Dai, L.; Yang, Y.; Li, J. Controlled Rod Nanostructured Assembly of Diphenylalanine and Their Optical Waveguide Properties. ACS Nano 2015, 9 (3), 2689–2695. https://doi.org/10.1021/acsnano.5b00623.